# Barcoded Metal Nanowires: Optical Reflectivity and Patterned Fluorescence†

**Sheila R. Nicewarner-Peña, Anthony J. Carado, Kristen E. Shale, and Christine D. Keating***

*Department of Chemistry, The Pennsylvania State University, University Park, Pennsylvania 16802*

*Received: January 17, 2003; In Final Form: April 3, 2003*

Metallic "barcodes" have been reported recently in which the size and location of distinguishable metal segments (e.g., Au and Ag) are used to encode information [Nicewarner-Peña et al., *Science* **2001**, *294*, 137−141]. Barcode readout is accomplished by conventional brightfield reflectance optical microscopy. Herein we report the wavelength-dependent optical reflectivity of individual stripes in metallic barcodes, and how this wavelength-dependence impacts the intensity of fluorescence from sandwich immuno- and hybridization assays performed on the particle surface. The encoded particles used in this study were striped nanowires on the order of 4−8 $\mu$m in overall length, with individual stripes typically on the order of 1−2 $\mu$m, and diameters ∼320 nm. Reflectivity measurements were made for several metals (Ag, Cu, Co, Ni, Pd, and Pt) relative to Au, which was used as an internal standard. Despite the subwavelength diameters of these nanowires, good agreement was found between experimentally determined reflectivities and bulk metal values. Under some conditions, fluorescence intensity patterns corresponding to the underlying metal segments could be observed. We find that the ratio of fluorescence intensities on different metal segments correlate with the metal reflectivity ratios at the excitation and emission wavelengths for the dye. Surface roughness and chemical effects may also play a role for some metals. We have shown that by choice of the underlying metal, particle striping patterns can be accentuated or hidden in the fluorescence image. This is demonstrated in a triplexed DNA hybridization assay.

## Introduction

Metal particles are known for their interesting and often useful optical and electrical properties. Observed properties are dramatically impacted by size, shape, and interparticle spacing.[1−3] For example, metal nanospheres tens of nanometers in diameter are intensely colored, due to surface plasmon absorbance,[1−3] while bulk metals are highly reflective.[4,5] The extinction spectra of small metallic nanowires exhibit two plasmon resonance features, corresponding to excitations along their long and short axes.[6−11] Such particles can be prepared by chemical reduction methods[12,13] or by electrodeposition within the pores of alumina or polycarbonate templates.[6−9,14] As nanowire length and/or width increases, scattering and reflectance become more intense. Nanowires several micrometers in length have been prepared by templated electrodeposition;[14] optical microscopy has been used to image these wires for diameters from 320 down to 30 nm.[15−20] Segmented nanowires composed of adjacent metallic stripes can also be prepared by this method.[15,17−20]

We recently reported the use of striped metal nanowires several micrometers long and ∼320 nm in diameter as "barcoded" particles for possible applications in multiplexed bioanalysis.[15] The metal striping pattern produced during synthesis is used to encode information such as the identity of a biomolecule bound to the nanowire surface; this pattern can be read out via simple reflectance microscopy.[15,18] Most of the literature on metal particles describes absorbance and scattering for much smaller nanowires or spheres; little has been reported on the optical properties of nanowires in this size range or having this level of compositional complexity.

Herein we describe the reflectivity for a variety of metals incorporated as 1 to 2 micrometer stripes in barcoded nanowires (overall dimensions ∼320 nm in diameter and 4−8 $\mu$m in length), and investigate fluorescence intensity as a function of underlying metal identity and fluorophore excitation/emission spectra. In fluorescence-based assays employing striped nanowires of this type, we had previously observed that the striping pattern was visible in the fluorescence image in some cases.[15,21] Here, we show that the striped fluorescence observed on barcoded nanowires correlates with the wavelength-dependent reflectivity of the underlying metals combined with the spectral properties of the fluorophore used.

For Au/Ag and Au/Pt striped nanowires, fluorophore surface coverage is very similar on the different metal segments. It is therefore possible, by appropriate choice of fluorophore and of metals for barcode stripes, to either accentuate or obscure the underlying striping pattern in fluorescence images. This is demonstrated in a triplexed DNA hybridization assay on barcoded Au/Ag nanowires, where three simultaneous sandwich hybridization assays are conducted on the nanowires, with fluorophores chosen to either visualize or obscure the particle striping pattern.

## Materials and Methods

**Materials.** Gold (Orotemp 24−1 troy oz/gal), silver (Silver 1025−4.5 troy oz/gal), nickel (Nickel S), copper (Cu U), and palladium (Pallaseed VHS 8 g/qt) plating solutions for nanowire synthesis were purchased from Technic, Inc. Pt and Co were electrodeposited from solutions prepared in house. Pt was electroplated from 0.01 M $H_2PtCl_6$ in 0.5 M $H_2SO_4$. Co was electroplated from 0.36 M $CoSO_4 \cdot 7\ H_2O$, 0.19 M $Na_3$citrate, and 0.1 M citric acid adjusted to pH 5 with 10.0 M NaOH. Ag wire (99.999%) and Ag shots for evaporation onto the backside of alumina membranes were purchased from Acros. A mini centrifuge with maximal relative centrifugal force (RCF): 2000*g* was purchased from VWR Scientific Products. Immersion oil ($n_D$ = 1.5150) for microscopy was purchased from Cargille Laboratories, Inc. Au finder grids were purchased from Electron

† Part of the special issue "Arnim Henglein Festschrift".

* Corresponding author. E-mail: keating@chem.psu.edu.

10.1021/jp034139i CCC: $25.00 
Published on Web 05/31/2003

**TABLE 1: Oligonucleotide Sequences Used in This Work**

| sequence number | sequence (5′ to 3′) | description |
|---|---|---|
| **Ia** | 5′-biotin−aaa AAA AAC TCC TTG CGC ACG T | 22-mer capture sequence 1 |
| **Ib** | CGT GCG TCA AAA ATT ACG TGC GGA AGG AGT T | 31-mer complementary to **I** |
| **Ic** | AAT TTT TGA CGC ACG-3′-fluor[a] | fluorophore labeled 15-mer for detection of **Ib** |
| **IIa** | 5′-biotin−aaa AAA ACG TTG TCT GAT GCG TCA | 24-mer capture sequence 2 |
| **IIb** | ACA CAG ACG TAC TAT CAT TGA CGC ATC AGA CAA CGT | 36-mer complementary to **II** |
| **IIc** | ATG ATA GTA CGT CTG TGT-3′-fluor[a] | fluorophore labeled 18-mer for detection of **IIb** |
| **IIIa** | 5′-biotin−aaa AAA CGA TAA CGG TCG GTA | 21-mer capture sequence 3 |
| **IIIb** | TAT GGC CAG CTC CCG TAC CGA CCG TTA TCG | 31-mer complementary to **III** |
| **IIIc** | CGG GAG CTG GCC ATA-3′-fluor[a] | fluorophore labeled 15-mer for detection of **IIIb** |
| **IV** | CGC ATT CAG GAT | 12-mer noncomplementary control |

[a] Two different fluorophores were used for oligonucleotide labeling: F = 6-carboxyfluorescein (6-FAM), $\lambda_{ex} = 495$ nm, $\lambda_{em} = 520$ nm; R = rhodamine-X (ROX), $\lambda_{ex} = 588$ nm, $\lambda_{em} = 608$ nm. Note that these $\lambda_{ex}$ and $\lambda_{em}$ values are essentially identical to those of FITC and Texas Red, respectively, which were used to label antibodies in this work.

Microscopy Sciences (200 mesh). The following chemicals were purchased from Calbiochem: α-rabbit IgG (H&L chain) monospecific for RIgG heavy and light chains conjugated to FITC or Texas Red, and α-rabbit IgG (Fc specific); both isolated from goat. Bovine serum albumin (BSA), α-globulin and protease-free, was purchased from Jackson Immuno Research Laboratories, Inc. Bis(3-aminopropyl)-terminated poly(ethylene glycol) [amino PEG] was purchased from Aldrich. NeutrAvidin was purchased from Pierce. Calf thymus DNA was purchased from Sigma. Oligonucleotides were purchased from Integrated DNA technologies, Inc (IDT). All $H_2O$ was distilled and purified to at least 18.2 MΩ through a Barnstead Nanopure system.

**Nanowire Synthesis.** Anodisc alumina membranes (25 mm diameter, Whatman) were used as templates for the synthesis of striped nanowires. The diameters of the pores were nominally 200 nm; however, SEM measurements of the membranes indicate that the pores widen in the membrane channel giving average diameters of 318 ± 50 nm.[14,22] These data are supported by transmission electron microscopy analysis of nanowires after removal from the templates. Synthesis of striped nanowires was performed on the basis of a modification of previously described methods[6−9,22,23] and has been described in detail elsewhere.[18] In brief, the backside (the side attached to the supporting ring) of an alumina membrane was coated with ∼500 nm of Ag by thermal evaporation. The membrane was then placed into an electrochemical cell where an additional ∼1 μm of Ag was electrodeposited onto the evaporated Ag film. This was done to ensure complete coverage of membrane pores and to prevent leakage during electrodeposition. Following Ag deposition, the membrane was removed from the cell, reversed, and placed back into the cell, pore side up, so that more Ag could be electrodeposited (−0.55 mA/cm$^2$ for 20 min) into the membrane. This step is included due to template irregularities near the membrane surface (smaller, interconnected pores); this region is filled with sacrificial Ag prior to nanowire deposition. By changing the plating solution at defined intervals for the metal of interest, the desired striping pattern was achieved. A variety of nanowire striping patterns were used in this work, including several different Au/Ag patterns, Au−X−Au where X = Co, Cu, Ni, Pt, or Pd, and Ni−Au−Ag. In general, widths as determined from TEM were ∼320 nm and overall lengths ranged from 4 to 8 μm, with each stripe ∼1 μm or longer. Exact particle and stripe dimensions varied from batch to batch within this range; within-batch standard deviations in nanowire length were on the order of 10%. When synthesis was complete, the cell was disassembled, and the membrane was removed and thoroughly rinsed with $H_2O$. The silver backing was dissolved by the addition of 4 M $HNO_3$ onto the evaporated Ag side of the membrane for 5 min after which the membrane was rinsed extensively with $H_2O$. The alumina membrane was dissolved by treatment with 3 M NaOH for 30 min, and the resulting nanowire suspension was centrifuged at 2000*g* for 30 s to collect the nanowires. The nanowires were resuspended and rinsed in $H_2O$ several times to remove residual base and salts. They were then washed at least three times in ethanol, and stored in this solvent until ready to use.

**Optical Microscopy.** Data were acquired on a Nikon TE-300 inverted microscope equipped with a Hamamatsu ORCA 12 bit high-resolution, 6.7 μm pixel, digital cooled CCD camera (1024 × 1024). Nanowires were imaged using a CFI Plan fluor 100× oil immersion lens (N.A. = 1.3), and Image-Pro Plus software. The excitation source for both fluorescence and reflected light images was a 100 W Hg lamp. Bioassay samples in aqueous solution were mounted between a glass slide and cover slip using a Secure-Seal spacer (Molecular Probes). Reflectance optical microscopy images were acquired using a Nikon bright field reflectance filter set containing a 50/50 beam splitter. Band-pass filters at 430, 490, 520, 580, and 600 ± 5 nm (Omega Optical) were used for wavelength selection. Underivatized striped rods used for reflectivity studies were dropped onto glass slides, dried under a light stream of argon, and coated with a drop of immersion oil followed by a coverslip for imaging.

For fluorescence images, samples were kept in the dark prior to imaging, and fluorescence images were taken before reflectivity images to prevent photobleaching. All exposure times were less than 1 s. Fluorescence images were obtained using Nikon filter cube sets. Two green and two red fluorophores were used in this work. Antibodies were labeled with either fluorescein isothiocyanate (FITC) or Texas Red (TR), while oligonucleotides were labeled with either 6-carboxyfluorescein (6-FAM) or rhodamine-X (ROX). FITC and 6-FAM have nearly identical excitation and emission maxima ($\lambda_{ex}$ and $\lambda_{em}$, respectively); fluorescence images for these probes were acquired using a Nikon FITC cube containing the following filters, excitation: 465−495 nm, dichroic: 505 nm, and emission: 515−555 nm. Texas Red (TR), and rhodamine-X (ROX) images were acquired using a Nikon "wide green" filter cube containing the following filters, excitation: 515−555 nm, dichroic: 565 nm, and emission: ≥ 590 nm.

**Electron Microscopy.** Field emission−scanning electron microscopy images (FE-SEM) were acquired for uncoated nanowire samples using secondary electron detection on a LEO 1530 FE-SEM.[18,24] Transmission electron microscopy (TEM) images were acquired on a JEOL 1200EXII located at the PSU Life Sciences Electron Microscope Facility.

**Sandwich Immunoassay Procedure.** An aliquot of nanowires (∼100 μL) was removed from the ethanolic stock solution, and rinsed twice in $H_2O$ (1 mL each rinse), and once in 50 mM Na phosphate buffer pH 7.2 (1 mL). Nanowires were derivatized

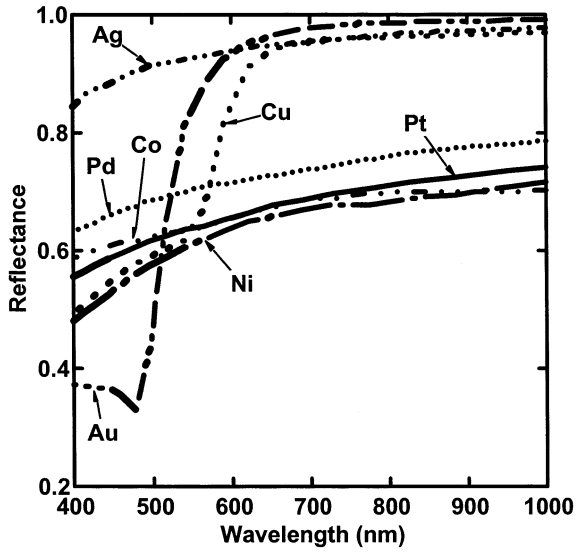


**Figure 1.** Wavelength-dependent reflectivity for bulk metals. Data plotted from ref 25.

with the capture antibody (α-RIgG Fc specific) by suspension into 500 μL of a 0.05 mg/mL solution. This was allowed to proceed for 1 h at room temperature, after which the samples were rinsed with 1 mL of the 50 mM Na phosphate buffer pH 7.2. Following direct adsorption of the capture antibody, nanowires were further derivatized with bis-aminated poly(ethylene glycol) (amino PEG) using a 1% solution of amino PEG in the 50 mM Na phosphate buffer. Following adsorption of amino PEG for 15 min., the nanowires were rinsed with 50 mM Na phosphate buffer three times (1 mL each rinse). Nonspecific sites on the capture antibody were blocked using a 1% solution of BSA in the 50 mM Na phosphate buffer pH 7.2. Blocking of the capture antibody was allowed to proceed for 15 min at room temperature, after which the nanowires were rinsed two times in the 50 mM Na phosphate buffer (1 mL each rinse), re-suspended into 500 μL of a 0.05 mg/mL solution of the analyte, RIgG, and allowed to react for 60 min at room temperature. Samples were rinsed with 1 mL of the 50 mM Na phosphate buffer. Nanowires were then re-suspended into ∼300 μL of the fluorescently labeled detection antibody, $\alpha\text{-RIgG}_{\text{H\&L}}$ FITC or Texas Red conjugate. Incubation with the detection antibody was allowed to proceed for 60 min at room temperature, after which the nanowires were rinsed three times in 500 μL of the 50 mM Na phosphate buffer. During adsorption of capture antibody, blocking steps, and incubation with the analyte and detection antibodies, samples were placed onto a vortexer, equipped with an attachment for holding eppendorf tubes. Samples were gently shaken in order to keep the nanowires suspended. Samples were also sonicated briefly (∼10−15 s) between rinsing steps to ensure good re-suspension of the nanowires and displacement from the eppendorf tube wall.

**Sandwich DNA Hybridization Assay.** Aliquots (600 μL) from each of three different barcoded nanowire patterns Ag−Ag−Au−Ag−Ag (**1**), Au−Ag−Au−Au−Au (**2**), and Au−Ag−Au−Ag−Au (**3**) were removed from the stock solutions stored in ethanol. The nanowires, each placed in different eppendorf tubes, were rinsed with 1 mL of $H_2O$ three times, then with 1 mL of 50 mM Na phosphate buffer pH 7.2, after which they were re-suspended into 1 mL of 0.05 mg/mL of NeutrAvidin (NA) in 50 mM Na phosphate buffer. The NA was allowed to adsorb onto the nanowire surface for 2 h at room temperature during gentle shaking. Following adsorption of NA, the nanowires were allowed to react with 500 mL of a 1%

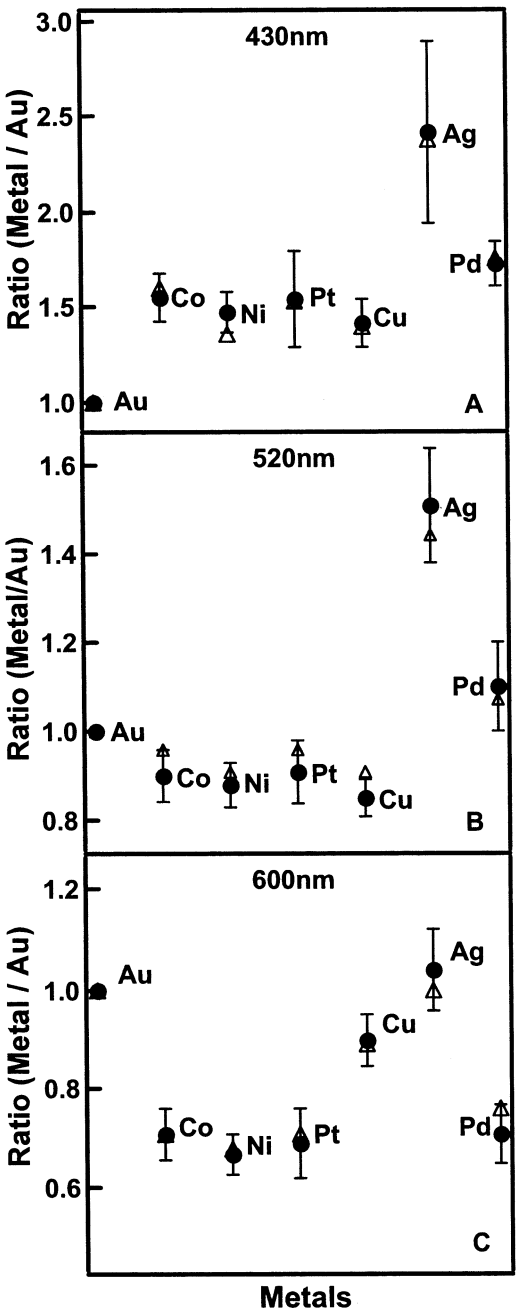


**Figure 2.** Ratio of reflected intensities for various metals vs Au for bulk materials (△) and striped particles (●) at 430 nm (A), 520 nm (B), and 600 nm (C). Experimental values were determined by reflectance optical microscopy.

solution of amino PEG in 50 mM Na phosphate buffer for an additional 15 min at room temperature, then rinsed twice with 1 mL of the 50 mM Na phosphate buffer. To provide specific capture chemistry for a solution-phase oligonucleotide (the analyte), nanowires of type **1**, **2**, and **3** were derivatized with a unique biotinylated oligo sequence **Ia**, **IIa**, and **IIIa**, respectively (Table 1 shows the DNA sequences used in this work). The nanowires were re-suspended into 1 mL of a 2 mM solution of the biotinylated oligo in 0.3 M NaCl/10 mM Na phosphate buffer pH 7.0. Binding of the biotinylated oligo with NA was allowed to proceed for 2 h at room temperature with gentle shaking. Following attachment of the biotinylated oligo, the samples were rinsed with 1 mL of the 0.3 M NaCl/10 mM Na phosphate buffer twice. Nanowires from all three reactions were mixed together and then separated into eight different aliquots

**TABLE 2: Ratio of Fluorescence and Reflectivity on Striped Particles**

| | observed intensity ratio[a] | bulk intensity ratio[b] |
|---|---|---|
| | Pt/Au Wires | |
| FITC fluorescence[c] | 0.98 ± 0.05 | |
| reflectivity @ 490 nm | 1.28 ± 0.11 | 1.42 |
| reflectivity @ 520 nm | 0.94 ± 0.07 | 0.96 |
| Texas Red fluorescence[c] | 0.60 ± 0.30 | |
| reflectivity @ 580 nm | 0.72 ± 0.08 | 0.71 |
| reflectivity @ 600 nm | 0.69 ± 0.07 | 0.71 |
| | Ag/Au Wires | |
| FITC fluorescence[b] | 2.21 ± 0.34 | |
| reflectivity @ 490 nm | 2.21 ± 0.23 | 2.08 |
| reflectivity @ 520 nm | 1.51 ± 0.13 | 1.44 |
| Texas Red fluorescence[c] | 1.00 ± 0.06 | |
| reflectivity @ 580 nm | 1.17 ± 0.24 | 1.01 |
| reflectivity @ 600 nm | 1.04 ± 0.08 | 1.00 |
| | Ni/Au wires | |
| FITC fluorescence[b] | 0.48 ± 0.43 | |
| reflectivity @ 490 nm | 1.05 ± 0.10 | 1.31 |
| reflectivity @ 520 nm | 0.88 ± 0.05 | 0.91 |
| Texas Red fluorescence[c] | 0.52 ± 0.13 | |
| reflectivity @ 580 nm | 0.65 ± 0.07 | 0.68 |
| reflectivity @ 600 nm | 0.67 ± 0.04 | 0.68 |

[a] Ratios are reported as M/Au, where M = Pt, Ag, or Ni. Reported reflectivity and fluorescence ratios are the average values ± standard deviation from approximately 50 particles, with intensities measured at three locations per metal within each particle. [b] Intensities listed are expected ratios based on bulk metal from Figure 1. [c] FITC $\lambda_{ex}$ = 494 nm, $\lambda_{em}$ = 518 nm. [c] Texas Red $\lambda_{ex}$ = 587 nm, $\lambda_{em}$ = 602 nm.

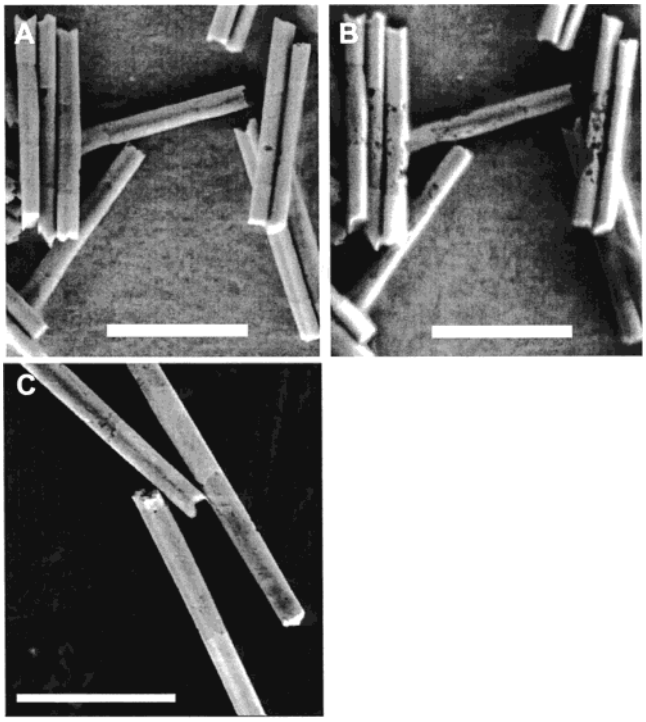


**Figure 3.** Ag degradation in underivatized Au−Ag−Au striped particles. FE-SEM images of as-prepared (A), and of the same particles after aging for 14 days in $H_2O$ (B). Similar effects were observed for particles stored dry in air. (C) Particles stored in ethanol for over 1 year prior to FE-SEM imaging. Scale bars are 2 $\mu$m.

for reaction to various combinations of the oligonucleotide analytes, **Ib**, **IIb**, and **IIIb**. An amount of 400 $\mu$L of a 2 mM solution of each analyte combination was used during the first hybridization step. For the control sample, which did not contain any analytes, 400 mL of hybridization buffer was used (hybridization buffer was 0.3 M NaCl/10 mM Na phosphate buffer pH 7.0). Analyte solutions were spiked with 2 mM of oligonucleotide sequence **IV** and 0.5 mg/mL calf thymus DNA to decrease nonspecific interactions between noncomplementary oligos. The first hybridization was allowed to proceed for 4 h at 40 °C, after which, the samples were rinsed with 1 mL of the hybridization buffer twice. Each of the samples was then separated into half for a total of sixteen reactions (this was necessary so that each reaction could be hybridized with both a 6-FAM labeled and ROX labeled detection oligo). The samples were re-suspended into 200 mL of a 2 mM mixture of all three detection oligos, **Ic-R** or **Ic-F**, **IIc-R** or **IIc-F,** and **IIIc-R** or **IIIc-F** that was spiked with 2 mM **IV** and 0.5 mg/mL calf thymus DNA. This second hybridization was allowed to proceed for 4 h at 40 °C. Following the second hybridization, the samples were rinsed in 1 mL of 1% SDS/0.3 M NaCl/10 mM Na phosphate buffer pH 7.0 solution. Then, 1 mL of 0.1% SDS/0.3 M NaCl/10 mM Na phosphate buffer, and a final rinse of 1 mL 0.3 M NaCl/10 mM Na phosphate buffer. During adsorption of NA and blocking with amino PEG, samples were placed onto a vortexer, equipped with an attachment for holding eppendorf tubes. Samples were gently shaken in order to keep the nanowires suspended. During hybridizations, samples were attached to a horizontal rotator (to keep the particles suspended in solution), which could be placed into a water bath. Samples were also sonicated briefly (∼10−15 s) between rinsing steps to ensure good re-suspension of the nanowires and displacement from the eppendorf tube wall.

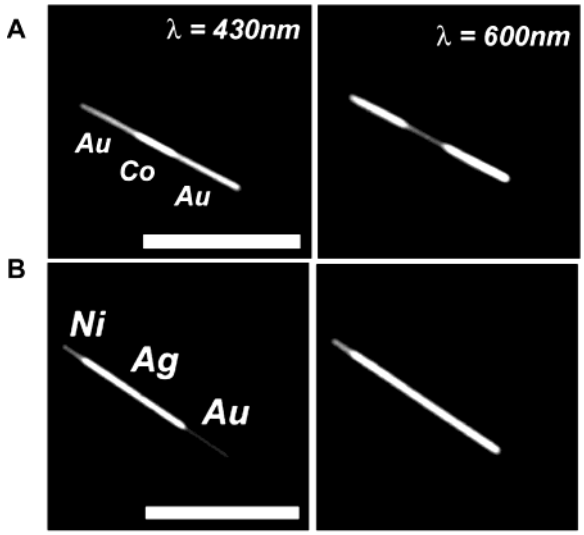


**Figure 4.** Optical reflectivity for striped rods with Co, Au, Ni, and Ag stripes. (A) Optical reflectivity image of an Au−Co−Au nanowire with 430 and 600 nm illumination. The Co segment is more reflective than the Au segment in the blue, but less reflective in the red. (B) Optical reflectivity image of Ni−Ag−Au wires with 430 and 600 nm illumination. The three metals can be distinguished by intensity at 430 nm and by their change in relative intensity when illuminated with 600 nm light. Scale bars are 5 $\mu$m.

## Results and Discussion

**Optical Characterization of Striped Particles.** The barcode patterns of striped nanowires are visualized by the differential reflectivity of adjacent metal stripes. We have reported that the reflectivity ratio at 430 nm illumination for segments within striped nanowires closely matches that for bulk metal.[15] Here, we further characterize the optical reflectivity of Au, Co, Ni, Pt, Cu, Ag, and Pd nanowire segments at several wavelengths. For this study, we prepared striped nanowires with 320 ± 30 nm diameter and several micrometers total length. To facilitate

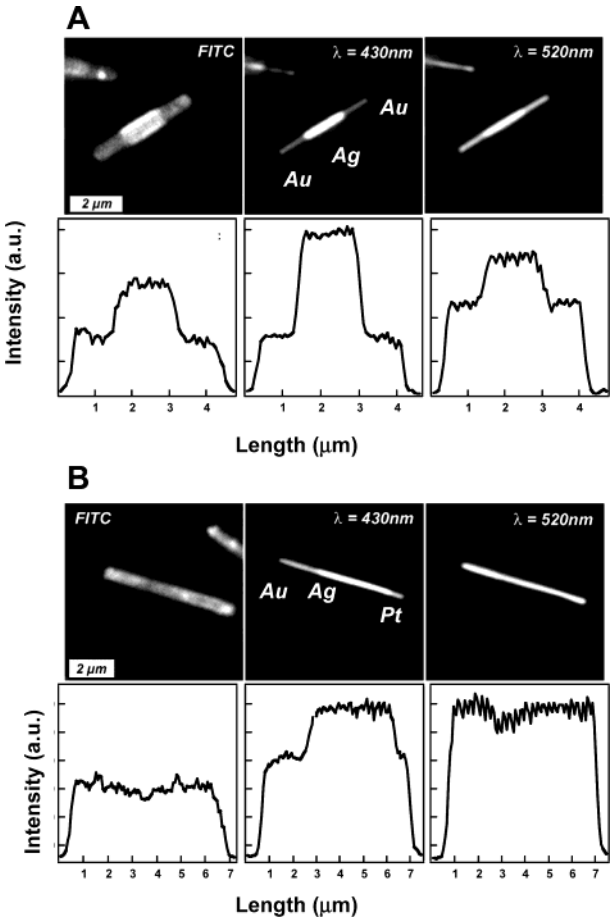


**Figure 5.** Fluorescence and reflectance optical microscopy images (top panels) and line profiles (bottom panels) of a sandwich immunoassay performed using FITC labeled α-RIgG on Au−Ag−Au particles (A) and on Au−Pt−Au particles (B). The particle striping pattern can be seen in the fluorescence image of A, while not in B.

quantitative comparison with bulk values, Au was used as an internal standard. Nanowires were synthesized such that the metal of interest was placed between two Au segments with the striping pattern Au−X−Au (where X denotes the metal of interest).

The wavelength-dependent reflectance for the bulk metals used (Au, Ag, Co, Pd, Pt, Cu, and Ni) is shown in Figure 1, plotted from values in ref 25. Experimentally determined reflectivity ratios for nanowire segments are plotted in Figure 2 along with values for the corresponding bulk metals. Reflectivities are plotted at 430, 520, and 600 nm as the ratio of intensity for the metal of interest to that of an adjacent Au segment, averaged from ≥50 particles of each striping type. Ratios for additional wavelengths are given in Table 2.

Agreement between 320 nm diameter, micrometer long metal stripes and bulk material is quite good; in most cases, experimentally obtained and bulk values are within one standard deviation. Irregularities in surface nanostructure contribute to the standard deviations in reflectivities for all metals. These features cannot be directly observed via optical microscopy but can be seen in electron micrographs. For Ag/Au at 430 nm, the error bars are quite large, presumably due to variations in surface roughness resulting from oxidation. Because Ag segments oxidize in air, the prior history of samples (age and storage conditions) can be important to their reflectivity. Figure 3 shows FE-SEM images of bare Au−Ag−Au nanowires (A) freshly prepared, and (B) the same nanowires after storage for 14 days in $H_2O$. The Ag segments become rough and pitted over time as a result of oxidation, while Au segments are unchanged. Similar results are observed for Ag-containing nanowires stored dry in air. In contrast, nanowires stored in ethanol are stable indefinitely; Figure 3C shows an FE-SEM image of Au−Ag−Au particles after 1 year in ethanol. Cu segments are much more susceptible to oxidation; damage is observable via optical microscopy after only 24 h storage in $H_2O$ (data not shown). Cu segments could be protected by storage in ethanol or dry under argon. Note that for the remainder of experiments described here, no special efforts were taken to avoid air oxidation; nanowires are routinely stored in ethanol prior to use, and in buffered $H_2O$ after derivatization with biomolecules.

The data in Figure 2 suggest the possibility of optically differentiating more than two metals in a single nanowire. While contrast between Ag and Au under blue illumination is the highest of any metal pair, other pairs of metals can be readily distinguished. Images of Au−Co−Au and Ni−Ag−Au nanowires are shown in Figure 4 (additional examples and wavelengths are available as Supporting Information). With 430 nm illumination, Co segments appear brighter than adjacent Au segments, while at 600 nm Au segments appear brighter, as expected based in Figures 1 and 2. Since the reflectivities of Co, Ni, Pd, and Pt are all quite similar (Figure 1), any of these metals can be incorporated as stripes in Au particles to give similar images. When Co, Pd, Pt, or Ni is incorporated in nanowires containing both Au and Ag, all three metals can be distinguished by imaging at 430 and 600 nm. While it is possible to identify all three metals by carefully evaluating reflectance intensities at a singe wavelength (e.g., 430 nm), the use of a second wavelength, i.e., 600 nm, enables unambiguous identification of the third metal. This can be seen in the bottom panels of Figure 4, which show an Ni−Ag−Au particle imaged at 430 and 600 nm. At 430 nm, Ag is brightest, followed by Ni and then Au. At 600 nm, Au and Ag segments have the same reflectivity, and the Ni segment can be readily identified. We have imaged multi-metal striped nanowires, e.g., Pt−Pd−Ni−Ag−Au, in which up to four of the different metal segments were distinguished at one wavelength.[15] Given the current error bars on segment reflectivity, four intensity levels (i.e., metals) in a single particle is impractical for multiplexing applications; however, improvements in nanowire synthesis, particularly if coupled with multiwavelength interrogation, may ultimately make four-metal striping patterns a realistic option.

**Patterned Fluorescence on Striped Particles.** One application for barcoded nanowires is as encoded, suspendable microsupports for multiplexed bioanalysis.[15,26] For this application, it is necessary not only to encode information (i.e., the type of bioassay being performed on each nanowire—for example, the sequence of DNA on the particle surface); it must also be possible to determine when a binding event has occurred. The most straightforward way to detect and/or quantitate bioassays on barcoded nanowires is using fluorescent tags in a sandwich-type format.[15] We had previously noted that nanowire striping patterns could be observed in fluorescence images for on-particle immuno- or DNA hybridization assays. This effect can be seen in Figure 5A, which shows a sandwich immunoassay on Au−Ag−Au nanowires. In this assay (lefthand panel of Scheme 1), a FITC labeled anti-rabbit immunoglobin (α-RIgG) was used for detection of RIgG binding to nanowire-bound antibodies specific for the Fc region of RIgG. The left panel of Figure 5 is a representative fluorescence optical microscopy image, while the middle and right panels are reflectance images taken using band-pass filters to reveal the metal striping pattern for this

**SCHEME 1: Schematic of Sandwich Assays Used in This Work**[a]

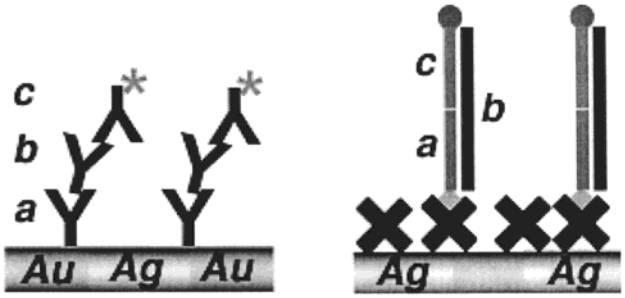


[a](*Left*) For immunoassays, the striped particles are first derivatized with a capture antibody, a, that is specific for the analyte, b, which is also an antibody. Following incubation of the capture antibody with the analyte, the fluorescently labeled detection antibody, c, was added. (*Right*) For hybridization assays, particles are derivatized with NeutrAvidin (NA, shown here as an X), followed by reaction with a biotinylated capture sequence, a, that is specific for a solution-phase analyte, b. Fluorescently labeled oligonucleotides, c, were then added for detection.

nanowire. The bright region in fluorescence correlates with the location of Ag metal in the nanowire, as can be seen from the reflectivity at 430 nm. The Ag/Au intensity ratio for the fluorescence image is similar to that for the reflectivity image taken at 520 nm, which is close to $\lambda_{em}$ for this fluorophore. When the same sandwich assay was repeated with Au and Pt as the underlying metals, much more uniform fluorescence was observed as shown in Figure 5B. The metal striping pattern, visible in the reflectivity image with 430 nm illumination, is not visible at 520 nm. These data indicate that the observed phenomena could be related to metal reflectivity near the fluorophore $\lambda_{em}$ and/or $\lambda_{ex}$. Other possibilities include differences in fluorophore surface coverage on the different metals, selective fluorescence quenching by Au segments, or roughness-induced enhancement on Ag segments. In the sandwich immunoassays performed here (Scheme 1A), the capture antibody is attached to the nanowire surface by direct, nonspecific adsorption. We would not expect dramatic differences in coverage between Au, Ag, and Pt surfaces under these conditions.

Fluorescence near metal surfaces is a well-studied phenomenon.[27−29] Two competing interactions, quenching and local field amplification (or enhancement), are observed. Quenching results from nonradiative energy transfer from the excited-state molecule to the metal surface, and varies as $d^{-3}$ where $d$ = distance from the metal surface.[30] Generally, quenching becomes important for distances very close to the metal surface, usually <ca. 10 nm.[28,31,32] The local field amplification also drops off with distance from the surface, but less steeply; thus, fluorescence intensities are increased for molecules on the order of 10−20 nm from the surface.[28,31] Optimal metal−molecule separation distances for surface-enhanced fluorescence (SEF) depend on the experimental system; a wide range of values has been reported.[27−29,33−36] For the assays used in this work (Scheme 1A), fluorophores were located far enough from the metal surface to minimize quenching (i.e., there were ∼3 layers of antibodies between the fluorophore and the nanowire surface which places the fluorophore ca. 15 nm from the metal).

Surface-enhanced fluorescence intensities depend not only on distance from the surface, but also on the morphology of the metal surface[37−39] and the quantum yield for the fluorophore.[40] Maximal enhancements are achieved in regions of high electromagnetic field amplification (such as occur near nanoscale surface features), and/or for fluorophores with low quantum yields. Smaller SEF effects are observed for smooth surfaces

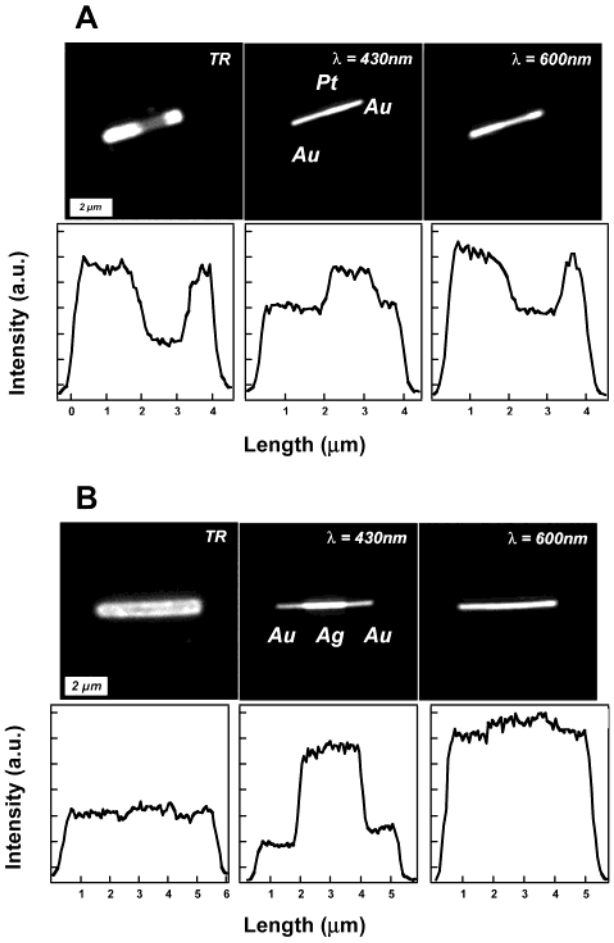


**Figure 6.** Fluorescence and reflectance optical microscopy images (top panels) and line profiles (bottom panels) of a sandwich immunoassay performed using TR labeled α-RIgG on Au−Pt−Au particles (A) and on Au−Ag−Au particles (B). The particle striping pattern can be seen in the fluorescence image of A, while not in B.

and/or fluorophores with high quantum yields. In our system,only high quantum yield fluorophores are used, and the morphology of the particles (320 nm diameter, ∼6 $\mu$m long cylinders) is not expected to give unusually high field amplifications. Thus, we do not expect a dramatic contribution from SEF in this system. However, the fluorophores are located in the near field (ca. 15 nm from the metal surface) and may experience different electromagnetic field enhancements above different stripes related to metal reflectivity.

To investigate the observed phenomenon further, the same sandwich assay was performed using TR labeled α-RIgG on the same Au−Pt striped nanowires, Figure 6A. This time, fluorescence was brighter on the Au segments as can be seen in the left panel. Again, the observation that fluorescence was brighter on certain metal segments correlated well with the reflectivities of the underlying metals. For this selection of metals (Au and Pt), Au is more reflective than Pt near the $\lambda_{ex}$ and $\lambda_{em}$ of TR. When the TR labeled immunoassay is performed on Au/Ag/Au nanowires, where the reflectivities are matched at $\lambda_{em}$, the striping pattern cannot be seen in the fluorescence image (Figure 6B). Together, these data suggest that striped fluorescence can be predicted on the basis of the relative reflectivities of the underlying metals.

Fluorescence and reflectance intensity ratios are compared quantitatively in Table 2.[41] If the observed uniform FITC fluorescence on Pt and Au segments is related to similar metal reflectivities near the $\lambda_{em}$ of FITC, which occurs at 518 nm,

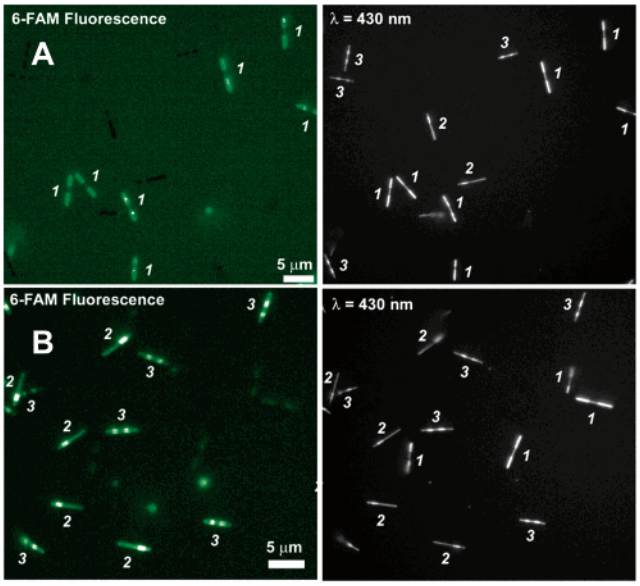


**Figure 7.** Fluorescence (left panel) and a reflectance optical microscopy image (right panel) of a multiplexed DNA hybridization using 6-FAM labeled detection oligos. The panels in A show the detection of a single analyte from solution while B shows the simultaneous detection of two analytes from solution. The particle striping pattern is clearly visible in the fluorescence image indicating that only the fluorescence image could be used to provide both analyte identity and presence. Scale bars are 5 $\mu$m.

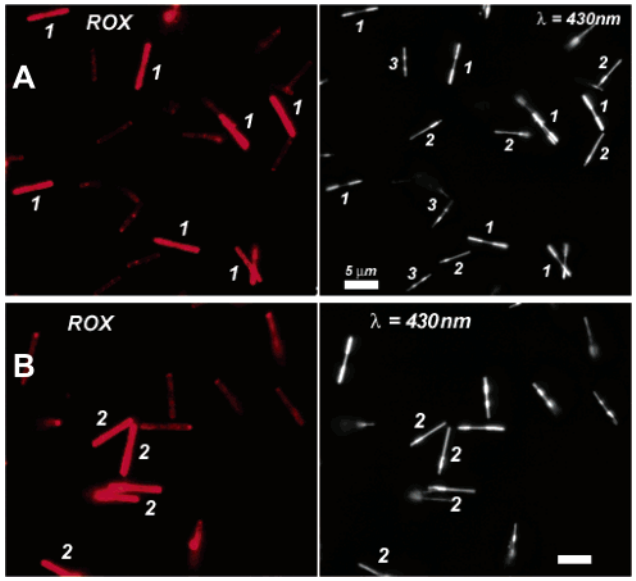


**Figure 8.** Fluorescence (left panel) and a reflectance optical microscopy image (right panel) of a multiplexed DNA hybridization using ROX labeled detection oligos. The panels in A show the detection of a single analyte from solution, while B shows the simultaneous detection of two analytes from solution. Particle striping pattern is not visible in the fluorescence image, indicating that both the fluorescence and reflectivity images are needed to provide analyte presence and identity, respectively. Scale bars are 5 $\mu$m.

then the expected ratio from the fluorescence intensity and the reflectivity intensity should be nearly identical. Indeed, that is what is observed. The intensity ratio for FITC is 0.98 ± 0.05, while the measured reflectivity ratio for Pt/Au at 520 nm is 0.94 ± 0.07. The increased fluorescence intensities for fluorophores located on more reflective metals is consistent with increased local fields above these metals.

Following this reasoning, the expected ratio for FITC on Au and Ag segments would be ~1.50 on the basis of the observed reflectivity ratio for Ag/Au at 520 nm. However, the measured FITC ratio is 2.21 ± 0.34, which is 1.5× higher. This may be due in part to additional electromagnetic field enhancement of FITC fluorescence by Ag at this wavelength due to surface roughness or to the greater reflectivity for Ag vs Au at $\lambda_{ex}$. Data for TR fluorescence indicate that any increase in Ag surface roughness does not significantly increase its surface area. Uniform TR fluorescence (ratio = 1.00 ± 0.06) is observed on Ag/Au rods, in agreement with nearly identical reflectivities at 600 nm (ratio = 1.04 ± 0.08).

Much larger deviations from expected fluorescence intensities are observed for nanowires composed of Au and Ni. The general trend of brighter fluorescence from Au vs Ni segments for both FITC and TR matches the reflectivity data at $\lambda_{em}$ for these fluorophores. However, in both cases the observed fluorescence ratios are considerably lower than the reflectivity ratios at $\lambda_{ex}$ or $\lambda_{em}$. This may indicate less efficient antibody adsorption on the Ni surface, perhaps due to surface oxidation of the Ni.

In summary, the data in Table 2 suggest that the observed fluorescence striping patterns can be predicted based on the relative reflectivities of the underlying metals. Since metal-fluorophore spacing was held constant in our experiments, and since data are acquired as *ratios* of intensity for fluorophores above adjacent segments, we cannot definitively attribute the observed effects to SEF phenomena. Indeed, a similar result might be expected for fluorophores located in the far field, where fluorescence patterning could arise not from increased local fields but rather from a wavelength-dependent mirror effect from the underlying substrate.

**DNA Hybridization on Striped Nanowires.** Patterned fluorescence has both advantages and disadvantages in bioanalysis. For example, it could be advantageous for streamlining bioassay analysis in that one image could be used for both analyte detection and nanowire identification. That is, instead of acquiring two images (a fluorescence image to determine presence of the analyte and a reflectivity image to reveal striping pattern), only one image would be needed to provide both analyte presence and striping pattern (which codes for a particular analyte). In addition, having segments with differing fluorescence intensities could potentially extend the dynamic range for detection. On the other hand, quantification is simplified by uniform brightness over an entire nanowire, and sensitivity is optimized by choosing $\lambda_{ex}$ and $\lambda_{em}$ to match high reflectivity regions for striping metals.

We have carried out multiplexed DNA hybridizations in which three different nanowire striping patterns of Au and Ag composition were used, each coding for a unique analyte (in this case a different oligonucleotide sequence). In parallel experiments, 6-FAM tagged and ROX tagged detection oligonucleotides were used for each analyte sequence. These fluorophores have nearly identical $\lambda_{ex}$ and $\lambda_{em}$ as the FITC and TR dyes used in the immunoassays described above. Scheme 1B illustrates the sandwich hybridization assay format used, in which three strands of DNA are involved in each of the three simultaneous analyses. The three unique capture sequences (**Ia**, **IIa**, and **IIIa**−**a** in the righthand panel of Scheme 1) were attached to nanowires of one of the three striping patterns: type **1** = Ag−Ag−Au−Ag−Ag (binary code 11011), type **2** = Au−Ag−Au−Au−Au (01000), and type **3** = Au−Ag−Au−Ag−Au (01010). Following derivatization, the nanowires were mixed together and hybridized with a mixture of the 3 analytes (**Ib**, **IIb**, and **IIIb**−**b** in Scheme 1). For detection, each possible combination of analyte mixture was then hybridized to a mixture of all three detection oligos, both FITC labeled and ROX

labeled. The detection sequences (**Ic-R** and **Ic-F**, **IIc-R** and **IIc-F**, and **IIIc-R** and **IIIc-F**) were each complementary to the second half of the analyte. Control experiments were also performed in which the analyte was omitted; the results showed virtually no background (data not shown). The results of the hybridization experiments are shown in Figures 7 and 8, in which a fluorescence image and a reflectivity image are shown for the detection of one or more analyte sequences in solution. To aid in the identification of the striping pattern, nanowires have been labeled (i.e., **1**, **2**, or **3**) in both the fluorescence and reflectivity images. Clearly, the striping pattern can be seen in the fluorescence image of Figure 7, however, not in Figure 8. Moreover, fluorescence is predominately observed from the intended particles (left panels of Figures 7 and 8), indicating that the specific capture sequences on the three nanowire types were able to selectively bind to their target oligo. These results demonstrate that multiplexed DNA hybridizations can be performed on barcoded nanowires such as these and that the reflectivity image was sufficient for the identification of the analyte oligo, as only one fluorophore was used in each experiment. Furthermore, the data also shows the possibility of using *only* the fluorescence image to determine both the presence of the analyte in solution and the identity of the analyte.

## Conclusions

The wavelength-dependent reflectivity for striped metal nanowires 320 nm in diameter has been determined for a variety of metals and compared to bulk metal. The quantitative data showed good agreement in all cases. We have shown that the phenomenon of striped fluorescence is related to differences in the wavelength-dependent reflectivities of the underlying metal segments. By appropriate choice of metals and fluorophores, it is possible to either accentuate or obscure this effect. For example, for bioassays in which quantitative information and high sensitivity are required, long-wavelength-excited fluorophores can be combined with Au and Ag striped nanowires to produce uniformly high fluorescence intensities. Alternatively, if shorter wavelength excitation/emission dyes are chosen, the striping pattern and presence/absence of analyte can be determined simultaneously in a single image.

**Acknowledgment.** We thank Prof. Vin Crespi for helpful discussions, and the National Institutes of Health (Grant HG02228) and The Pennsylvania State University for financial support of this research.

**Supporting Information Available:** In addition to the images of Au−Co−Au and Ni−Ag−Au nanowires shown in Figure 4, additional examples and wavelengths are available as Supporting Information. This material is available free of charge via the Internet at http://pubs.acs.org.

**Note Added after ASAP Posting.** This article was posted ASAP on the Web on 5/31/2003. Changes were made to the labels in Figure 5A. The correct version was posted on 6/09/2003.

## References and Notes

(1) Mie, G. *Ann. Phys.* **1908**, *25*, 377.
(2) *Colloidal Gold: Principles, Methods, and Applications*; Academic Press: San Diego, 1989; Vol. 1.
(3) Kreibig, U.; Vollmer, M. *Optical Properties of Metal Clusters*; Springer: New York, 1995.
(4) Kittel, C. *Introduction to Solid State Physics*, 7th ed.; Wiley: New York, 1996.
(5) Raether, H. *Surface Plasmons on Smooth and Rough surfaces and on Gratings*; Springer-Verlag: Berlin, 1988.
(6) Hornyak, G. L.; Patrissi, C. J.; Martin, C. R. *J. Phys. Chem. B* **1997**, *101*, 1548−1555.
(7) Foss, C. A., Jr.; Hornyak, G. L.; Stockert, J. A.; Martin, C. R. *J. Phys. Chem.* **1994**, *98*, 2963−2971.
(8) Foss, C. A., Jr.; Tierney, M. J.; Martin, C. R. *J. Phys. Chem. B* **1992**, *96*, 9001−9007.
(9) Foss, C. A., Jr.; Hornyak, G. L.; Stockert, J. A.; Martin, C. R. *J. Phys. Chem. B* **1992**, *96*, 7497−7499.
(10) Link, S.; Mohamed, M. B.; El-Sayed, M. A. J. *Phys. Chem. B* **1999**, *103*, 3073−3077.
(11) Preston, C. K.; Moskovits, M. *J. Phys. Chem. B* **1993**, *97*, 8495−8503.
(12) (a) Murphy, C. J.; Jana, N. R. *Adv. Mater*. **2002**, *14*, 80−82. (b) Jana, N. R.; Gearheart, L.; Murphy, C. J. *J. Phys. Chem. B* **2001**, *105*, 4065−4067.
(13) Brown, K. R.; Walter, D. G.; Natan, M. J. *Chem. Mater*. **2000**, *12*, 306−313.
(14) Martin, C. R. *Chem. Mater*. **1996**, *8*, 1739−1746.
(15) Nicewarner-Peña, S. R.; Freeman, R. G.; Reiss, B. D.; He, L.; Peña, D. J.; Walton, I. D.; Cromer, R.; Keating, C. D.; Natan, M. J. *Science* **2001**, *294*, 137−141.
(16) Martin, B. R.; St. Angelo, S.; Mallouk, T. E. *Adv. Funct. Mater*. **2002**, *12*, 759−765.
(17) Mock, J. J.; Oldenburg, S. J.; Smith, D. R.; Schultz, D. A.; Schultz, S. *Nano Lett*. **2002**, 2, 465−469.
(18) Reiss, B. D.; Freeman, R. G.; Walton, I. D.; Norton, S. M.; Smith, P. C.; Stonas, W. G.; Keating, C. D.; Natan, M. J. *J. Electroanal. Chem*. **2002**, *522*, 95−103.
(19) Dickson, R. M.; Lyon, L. A. *J. Phys. Chem. B* **2000**, *104*, 6095−6098.
(20) Martin, B. R.; Dermody, D. J.; Reiss, B. D.; Fang, M.; Lyon, L. A.; Natan, M. J.; Mallouk, T. E. *Adv. Mater*. **1999**, *11*, 1021−1025.
(21) Walton, I. D.; Norton, S. M.; Balasingham, A.; He, L.; Oviso, D. F.; Gupta, D.; Raju, P. A.; Natan, M. J.; Freeman, R. G. *Anal. Chem*. **2002**, *74*, 2240−2247.
(22) Hulteen, J. C.; Martin, C. R. *J. Mater. Chem.* **1997**, *7*, 1075−1085.
(23) Al-Mawlawi, D.; Liu, C. Z.; Moskovits, M. *J. Mater. Res.* **1994**, *9*, 1014−1018.
(24) Grabar, K. C.; Brown, K. R.; Keating, C. D.; Stranick, S. J.; Tang, S.-L.; Natan, M. J. *Anal. Chem.* **1997**, *69*, 471−477.
(25) *CRC Handbook of Chemistry and Physics*, 71st ed.; CRC Press: Cleveland: OH, 1990.
(26) For other types of encoded particles, see: (a) Cao, Y. C.; Jin, R.; Mirkin, C. A. *Science* **2002**, *297*, 1536−1540. (b) Nam, J.-M.; Park, S.-J.; Mirkin, C. A. *J. Am. Chem. Soc*. **2002,** *124*, 3820−3821. (c) Bruchez, M., Jr.; Moronne, M.; Gin, P.; Weiss, S.; Alivisatos, A. P. *Science* **1998**, *281*, 2013−2016. (d) Chan, W. C. W.; Nie, S. *Science* **1998**, *281*, 2016−2018. (e) Han, M.; Gao, X.; Su, J. Z.; Nie, S. *Nature Biotechnol.* **2001**, *19*, 631−635. (f) Ni, J.; Lipert, R. J.; Dawson, G. B.; Porter, M. D. *Anal. Chem*. **1999**, *71*, 4903−4908. (g) Schultz, S.; Smith, D. R.; Mock, J. J.; Schultz, D. A. *Proc. Natl. Acad. Sci*. **2000**, *97*, 996−1001. (h) Dunbar, S. A.; Jacobson, J. W. *Clin. Chem*. **2000**, *46*, 1498−1500. (i) Walt, D. R. *Science* **2000**, *287*, 451−452. (j) Battersby, B. J.; Bryant, D.; Meutermans, W.; Matthews, D.; Smythe, M. L.; Trau, M. *J. Am. Chem. Soc*. **2000**, *122*, 2138−2139.
(27) Moskovits, M. *Rev. Mod. Phys.* **1985**, *57*, 783−826.
(28) Neumann, T.; Johansson, M.-L.; Kambhampati, D.; Knoll, W. *Adv. Funct. Mater*. **2002**, *12*, 575−586.
(29) Metiu, H. *Prog. Surf. Sci.* **1984**, *17*, 153−320.
(30) Campion, A.; Gallo, A. R.; Harris, C. B.; Robota, H. J.; Whitmore, P. M. *Chem. Phys. Lett.* **1980**, *73*, 447−450.
(31) Pockrand, I.; Brillante, A.; Mobius, D. *Chem. Phys. Lett.* **1980**, *69*, 499−504.
(32) Kittredge, K. W.; Fox, M. A.; Whitesell, J. K. *J. Phys. Chem B* **2001**, *105*, 10594−10599.
(33) Wokaun, A.; Lutz, H. P.; King, A. P.; Wild, U. P.; Ernst, R. R. *J. Chem. Phys.* **1983**, *79*, 509−514.
(34) Tarcha, P. J.; DeSaja-Gonzalez, J.; Rodriguez-Llorente, S.; Aroca, R. *Appl. Spectrosc.* **1999**, *53*, 43−48.
(35) Knobloch, H.; Brunner, H.; Leitner, A.; Aussenegg, F.; Knoll, W. *J. Chem. Phys.* **1993**, *98*, 10093−10095.
(36) Kummerlen, J.; Leitner, A.; Brunner, H.; Aussenegg, F. R.; Wokaun, A. *Mol. Phys.* **1993**, *80*, 1031−1046.
(37) Amos, R. M.; Barnes, W. L. *Phys. Rev. B* **1999-I**, *59*, 7708−7714.
(38) (a) Chumanov, G.; Sokolov, K.; Gregory, B. W.; Cotton, T. M. *J. Phys. Chem.* **1995**, *99*, 9466−9471. (b) Sokolov, K.; Chumanov, G.; Cotton, T. M. *Anal. Chem*. **1998**, *70*, 3898−3905.
(39) Glass, A. M.; Liao, P. F.; Bergman, J. G.; Olson, D. H. *Opt. Lett*. **1980**, *5*, 368−370.
(40) Weitz, D. A.; Garoff, S.; Gersten, J. I.; Nitzan, A. *J. Chem. Phys.* **1983**, *78*, 5324−5338.
(41) Note that since these data are intensity ratios between the different metals, any change in absolute fluorescence intensities that is uniform across the metal segments will not be detected.